IEEE Access
Multidisciplinary | Rapid Review | Open Access Journal

Received December 29, 2020, accepted January 23, 2021, date of publication January 27, 2021, date of current version March 18, 2021.

Digital Object Identifier 10.1109/ACCESS.2021.3054920

Optimal Design of PMa-SynRM for Electric Vehicles Exploiting Adaptive-Sampling Kriging Algorithm

JI-CHANG SON[1], JONG-MIN AHN[1], JAEWON LIM[2], (Member, IEEE), AND DONG-KUK LIM[1], (Member, IEEE)

[1]School of Electrical Engineering, University of Ulsan, Ulsan 44610, South Korea
[2]System Engineering Research Division, Department of AI Machinery, Korea Institute of Machinery & Materials (KIMM), Daejeon 305-343, South Korea

Corresponding author: Dong-Kuk Lim (ldk8745@ulsan.ac.kr)

This work was supported by the National Research Foundation of Korea (NRF) grant by the Korean Government through the Ministry of Science and ICT under Grant 2019R1F1A1061132.

ABSTRACT Motor design can be said as multi-modal optimization problem, as many performances should be considered. In addition, a time-consuming finite element method (FEM) is required for accurate analysis of the motor, and such computational burden becomes worse when the FEM is applied to multi-modal optimization problem. In this paper, adaptive-sampling kriging algorithm (ASKA) is proposed to relieve the computation cost of multi-modal optimization problem. The ASKA utilizes kriging interpolation model with generated samples by Compact Search Sampling (CSS) and Exclusive Space-filling Method (ESM). The CSS improves the accuracy of the solutions by generating samples near the expected solutions, and the ESM guarantees the diversity of solutions by generating samples far from existing samples, avoiding solution-near area. Using CSS and ESM, the ASKA adjusts the number of samples effectively and reduces function call considerably. The superior performance of the ASKA was verified by mathematical test functions with complex objective function regions. To validate the feasibility of actual electric machines, the ASKA was applied to optimal design of permanent magnet assisted synchronous reluctance motors for electric vehicles and optimum design with diminished torque ripple is derived.

INDEX TERMS Electric vehicles, kriging, multi-modal optimization, optimal design, permanent magnet assisted synchronous reluctance motor (PMa-SynRM).

I. INTRODUCTION

Recently, in order to satisfy the strengthened environmental regulations due to excessive emission of greenhouse gases, interests in eco-friendly vehicles such as electric vehicles (EVs) have been increasing and many studies have been conducted on EVs. As motors for EV propulsion require high-power density, high efficiency, and mechanical stability at high-speed operation, the interior permanent magnet synchronous motor (IPMSM) has been widely used for EVs owing to high torque density, superior power factor, and efficiency by using both magnet torque and reluctance torque [1], [2]. However, the IPMSMs have problem with irreversible demagnetization of Nd-Fe-B magnets at high temperature, and high production cost due to recent increase in rare earth permanent magnet [3], [4]. The permanent magnet assisted synchronous reluctance motor (PMa-SynRM) uses ferrite magnet, and magnet is embedded inside the rotor core. The PMa-SynRM is an attractive alternative as it has cost competitivity on the aspect of utilizing ferrite magnet [5]. Also, multi-segmented and multi-layered structure of the magnets and usage of reluctance torque can compensate the diminution in the torque of the PMa-SynRM, which is caused by the usage of ferrite magnet [6].

However, as the PMa-SynRM utilizes both reluctance torque and magnet torque, it has problem with torque pulsation such as torque ripple, which causes vibration and noise to motor [7]. Since lower torque ripple leads to improved control stability and ensures comfortable driving, the motors for EVs should have lower torque ripple [8]. The torque ripple

The associate editor coordinating the review of this manuscript and approving it for publication was Sudhakar Babu Thanikanti.

depends on the shape of the motor, and the objective function region according to the shape represents complex shape with multiple solutions.

Moreover, finite element method (FEM) is essential for precise electromagnetic analysis of the motor due to nonlinear magnetic saturation characteristic of permanent magnet [9]. However, the FEM takes enormous amount of time and function call, specifically when applied to multi-modal optimization problems. Therefore, the multi-modal optimization algorithm that reduces the number of function calls, is essential.

To handle with multi-modal optimization problem and to remedy problem related to computational cost and improve convergence characteristic, this paper proposes Adaptive-Sampling Kriging Algorithm (ASKA). The ASKA applies kriging interpolation model which has lower computation time compared with standard approach [10]. The ASKA has Compact Search Sampling (CSS) step to enhance convergence characteristic and Exclusive Space-filling Method (ESM) step to reduce missing local minima. These two steps allow ASKA to find both global and local solutions with a small number of function calls.

The ASKA is tested on two mathematical test functions, and the validity of the ASKA is confirmed by comparison with three conventional stochastic optimization algorithms. Furthermore, purposed algorithm is verified by successfully drawing optimum design that reduces torque ripple when applied to optimal design of PMa-SynRM for EVs. Particularly, to relieve torque pulsation, noise, and vibration of the model, skewed rotor structure is applied [11], [12]. Moreover, whenever the structure is changed, a step finding current phase angle that has maximum torque is added to algorithm. Finally, the analysis of mechanical stress at maximum speed is conducted on optimum model to confirm that the motor is safe from breakage.

II. PROPOSED ALGORITHM

As a method of analyzing motor, two analysis methods are typically used, magnetic equivalent circuit method (MEC) and FEM. MEC model offers a good compromise between accuracy and computational cost [13]. In contrast, FEM guarantees accurate result and takes huge computational burden [14]. However, when it comes to optimal design of electric machines such as motors, analyzing precise characteristic is essential, as most electric machines have nonlinear magnetic saturation.

As mentioned before, the problem with FEM is computational time, and it takes tremendous amount of time, especially when applied to optimal design of electric machines. Furthermore, since the objective function region according to shape of motor has complex shape with many local peaks, an optimization algorithm that finds both global solution and local solutions with fewer function calls, is required.

Many heuristic optimization algorithms such as immune algorithm (IA) and niching genetic algorithm (NGA) have been proposed to deal with multi-modal optimization problem [15]–[18]. However, conventional heuristic algorithms still take unnecessary function calls when converge to peaks [19]. When combining the optimization algorithm with FEM, reduction of the number of function calls is necessary to minimize computational time. Therefore, this paper proposes algorithm that can enormously reduce the computation time and function calls.

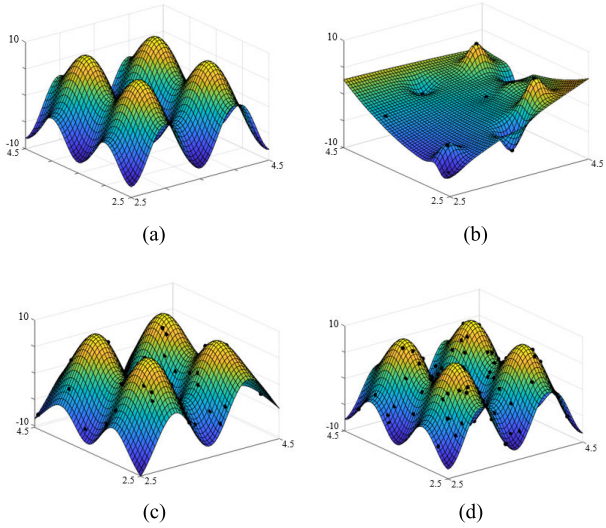

FIGURE 1. Three-dimensional plot of objective function region. (a) Real problem region. (b) Surrogate model with 15 samples. (c) Surrogate model with 45 samples. (d) Surrogate model with 100 samples.

The ASKA is an algorithm that proceeds based on the approximate models to reduce computational times considerably [20]. The approximate model is generated by predicting the values of the grid on the problem area, which is divided by N × N, using existing samples. The ASKA adopts kriging interpolation method, as it is known as an effective method to approximate a complex and nonlinear function [21]. Using kriging interpolation method, rough objective function region could be estimated with given samples. Figure 1 shows three-dimension plot of real objective function and surrogate model generated with different number of samples. The objective function of Figure 1(a) is defined as

$$f(x, y) = 5\cos(2\pi(x - 3)) + 3\cos(2\pi(y - 7)) \qquad (1)$$

where, $2.5 \leq x, y \leq 4.5$. Figure 1(c) is a picture of surrogate model generated with 45 samples, and it seems that approximate peak can be expected even with a small number of function calls. However, as shown in Figure 1(b), if the number of samples is insufficient, the correct objective function region cannot be interpolated. Moreover, when samples are generated more than necessary like in Figure 1(d), the accuracy of the solution is hardly increased due to saturation, wasting surplus function calls. Figure 2 clearly shows problem of kriging method regarding the number of samples. When the number of samples is not enough, error rate of the surrogate model drastically increases. Besides, when the number of samples exceed 50, which is regarded enough, accuracy of the surrogate model hardly improves. There-

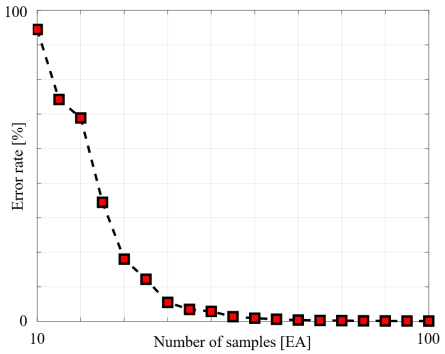

FIGURE 2. Error rate of kriging model on the peak point according to number of samples.

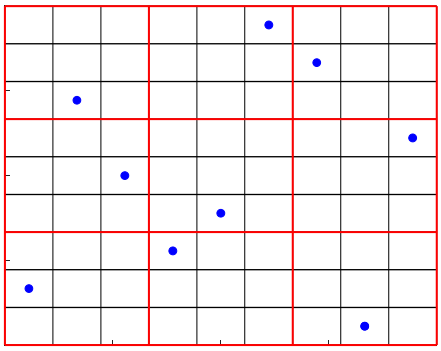

FIGURE 3. Conceptual schematic of Multi-Jittered Sampling.

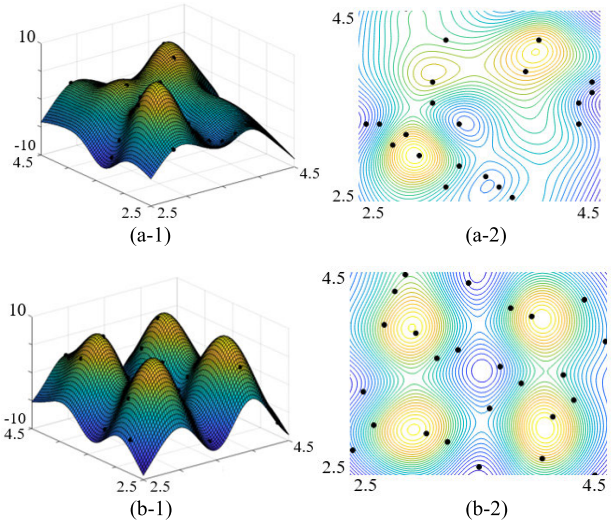

FIGURE 4. Three-dimensional plot and contour plot of kriging surrogate model. (a) Using random sampling. (b) Using MJS method.

fore, when using kriging method, determining the appropriate number of samples is required, and problem with determining proper number of samples occurs when objective function is unclear.

Many studies have been tried using kriging method and the error of the real problem area and surrogate model [22]–[24]. However, in the optimization of the electric machines, it seems more efficient to concentrate on finding more accurate solutions with a small number of function calls than to obtain a reliable surrogate model throughout entire objective function region. The proposed algorithm approaches the sample-generating problem on the aspect of enhancing accuracy of solution and eliminating missing local minima. The ASKA deal with such problem by automatically adjusting the number of generated samples effectively using CSS and ESM, and at the same time reduces function call drastically.

A. MULTI-JITTERED SAMPLING

The ASKA utilizes the Multi-Jittered Sampling (MJS) as a method to generate initial samples. For effective initial sampling, it is important to sample as evenly as possible while maintaining randomness [21], [25]. Firstly, the entire objective region is divided into N × M sub region, which is red box on Figure 3 when both N and M is 3. At one subregion, only one sample should be generated, to generate samples evenly. Then, the sub-region is divided again into N × M grid, which is marked as black lines on Figure 3. To maintain randomness, the samples are generated avoiding duplication at the same rows and columns. Figure 4 shows three-dimension plot and contour plot of the kriging surrogate model of random sampling and MJS when the objective region is defined as (1), and the number of samples are equal as 25. Comparing Figure 1(a), it is definite that the MJS has superior performance when applied to kriging interpolation method.

B. COMPACT SEARCH SAMPLING

The CSS is the step that improves the accuracy of the solutions of the kriging surrogate model by generating samples near the solutions: one on the predicted solution, and the other one among the points of first contour surrounding the predicted solutions. To execute CSS, contour information of the surrogate model is exploited, which is derived using MATLAB's contour function [26]. With the CSS, accurate solution can be found with fewer samples compared with scattering samples throughout the entire problem region.

First, rough surrogate model is made with existing samples, and the contour information of surrogate model is obtained. Using contour information, predicted solutions can be easily gotten, comparing each grid values of surrogate model. One CSS sample is added on the predicted solution, as it is calculated value. Also, from the contour information, the points that surrounding the solutions can be obtained, which are candidates of another CSS sample, and CSS sample is selected randomly among them. As the values of two points are calculated, additional function calls are required to both points.

In detail, Figure 5 shows the example of generating CSS sample. On the left, the contour background is drawn with kriging surrogate model that is generated by samples, which is black dots. On the right, point on the solution, which is obtained by calculation, is selected as CSS sample, and another CSS sample is selected among the candidates, on the first contour line near the solution.

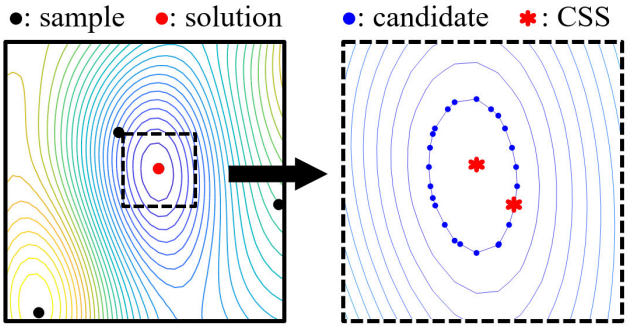

FIGURE 5. Example of generating CSS sample.

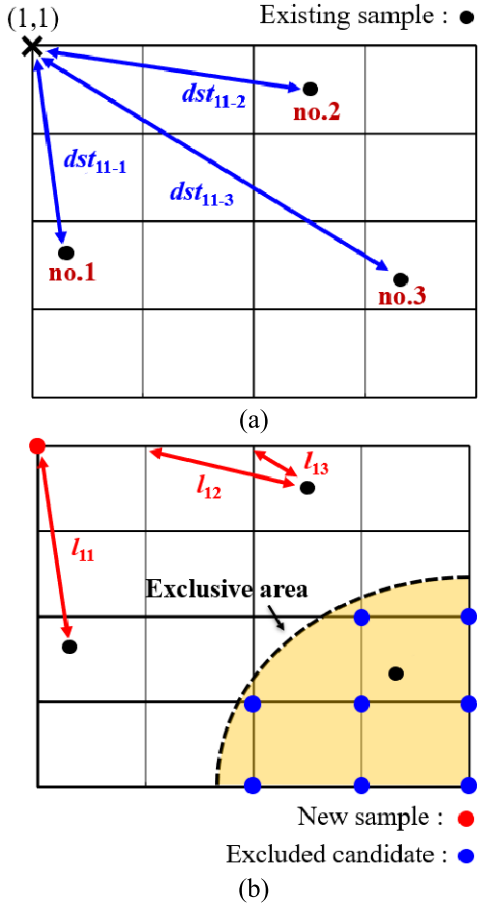

FIGURE 6. Conceptual Schematic of Exclusive Space-filling Method. (a) Calculation of distance from lattice point (1, 1) to existing samples. (b) Mutant generation considering distance and exclusive area.

C. EXCLUSIVE SPACE-FILLING METHOD

To maximize the ability to search missing local solutions and ensures the diversity of solutions, the ASKA adopts ESM as a method to generate mutant. Conventional space-filling method utilizes distance of grids on the objective region and existing samples and generates additional sample on the farthest grid from existing samples. On Figure 6(a), the black grid is dividing whole objective region and the lattice points are the candidates of new sample. First, the distance from each lattice point to existing samples is calculated, which is marked as $dst_{\text{ij-p}}$, where i and j denote the number of lattice point and p is the number of existing samples. The nearest length of each lattice point, marked l_{ij}, where i and j is the number of lattice point, is set by comparing $dst_{\text{ij-p}}$. The nearest length of lattice point (1,1) is $dst_{11\text{-}1}$. Finally, the additional sample is generated on the lattice point that has the maximum l_{ij} which means the farthest point from existing samples. When one sample is added, all the steps are repeated including the newly generated sample, until the number of mutants satisfies the requirement.

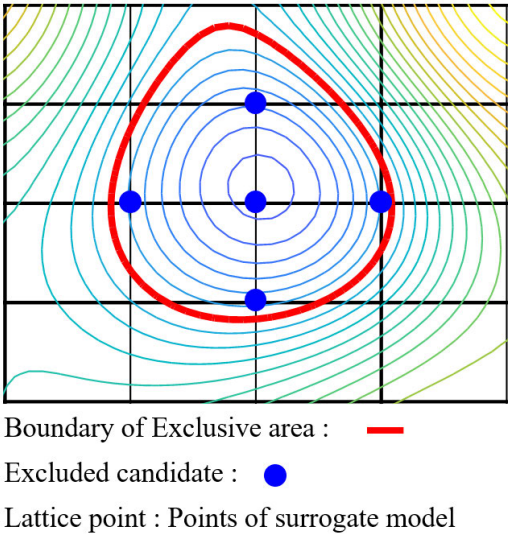

FIGURE 7. Setting of Exclusive area.

The difference of the ESM and conventional space-filling method is that the ESM exclude some candidates among lattice points, which are included in the sample-existing area. To classify the sample-existing area, the ESM uses contour information of surrogate model. As shown in Figure 7, the boundary of exclusive area is marked red and defined as the farthest contour enclosing the expected solutions. When the boundary is set, the lattice points inside of sample-existing area are excluded at the candidate. For example, on the right side of Figure 6, additional sample is generated on the grid with maximum l_{ij}, except the lattice point that (i, j) are (3, 4), (3, 5), (4, 3), (4, 4), (4, 5), (5, 3), (5, 4), and (5, 5). Instead of sampling throughout whole area, the ESM can also reduce the number of function call by preventing overlap sampling on the sample-existing area.

D. FLOW CHART OF THE ASKA

The flow chart of the ASKA is shown in Figure 8. The specific process of the proposed algorithm is as follows.

Step 1 (Problem Definition): Objective function, restrictions, and parameters are set.

Step 2 (Initial N Sample): Initial samples are generated over the entire objective function region. All the samples are generated with the MJS to derive approximate objective region. N means the number of samples.

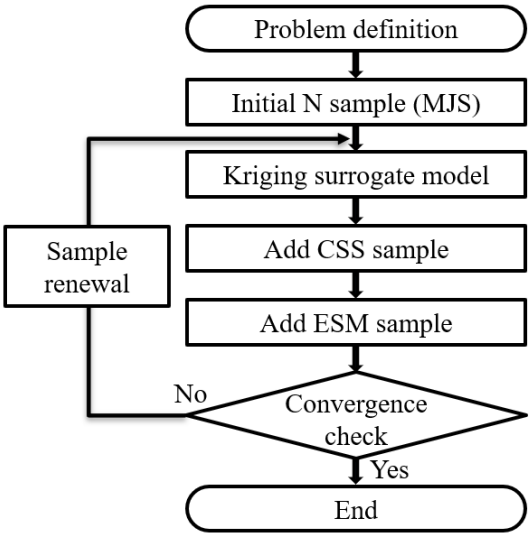

FIGURE 8. Flow chart of the ASKA.

Step 3 (Kriging Surrogate Model): Kriging surrogate model is made by existing N samples. No additional function call is required for generating interpolation model.

Step 4 (Add CSS Sample): Two CSS samples are generated near all solutions of kriging surrogate model. One is generated on the expected solution, and another one is selected among points of first contour line.

Step 5 (Add ESM Sample): Using kriging surrogate model contour information, the exclusive boundary is set around each solution. Mutants are generated on the farthest lattice point from the existing samples, except the lattice point that are inside of exclusive area.

Step 6 (Convergence Check): If the convergence condition is not met, sample group is updated with newly generated samples and existing samples. Continuously, each step is repeated from step 3, and algorithm proceeds with changed number of samples N. Else, algorithm is terminated and the global and solutions are derived.

E. VERIFICATION OF THE ALGORITHM

To verify the proposed algorithm, conventional multi-modal optimization algorithms, such as IA and NGA using restricted competition selection, similar sampling-based kriging algorithm using Latin hypercube sampling (LHS), and ASKA were applied to the optimization of two mathematical test functions [27]. For the LHS, the number of generated samples are set as equal to ASKA, and criteria of test is success rate. As shown in Figure 9, two test functions have complex objective region with multiple peaks, and are defined as

$$f_1(x,y) = \sum_{i=1}^{N_1} \frac{b_i}{1+[(x-x_i)^2+(y-y_i)^2]/a_i} \tag{2}$$

$$f_2(x,y) = \sum_{k=1}^{N_2} \frac{b_k}{1+[(x-x_k)^2+(y-y_k)^2]/a_k} \tag{3}$$

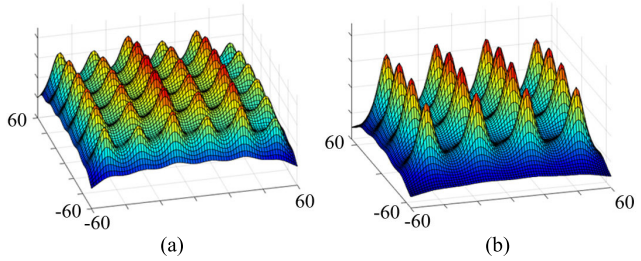

FIGURE 9. Three-dimensional plot of test functions. (a) Test function 1 with 36 peaks. (b) Test function 2 with 16 peaks.

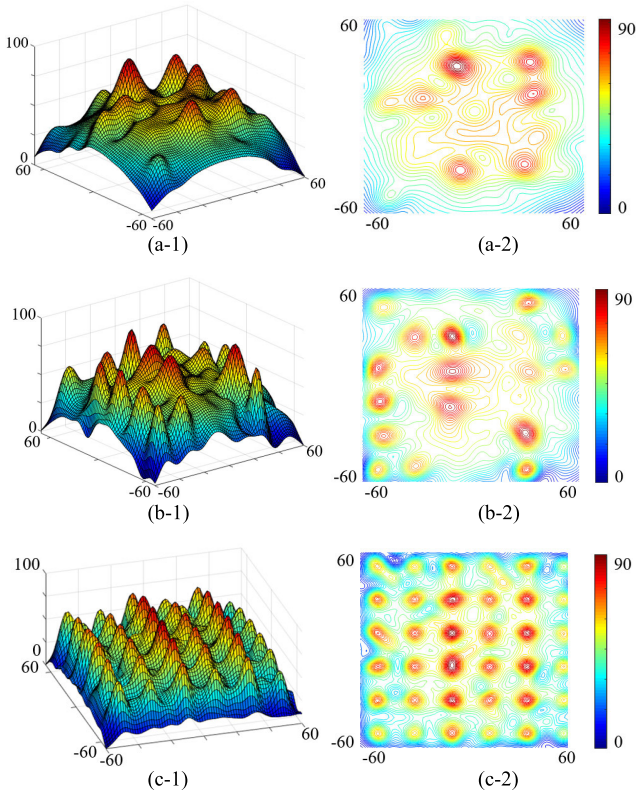

FIGURE 10. Optimization progress result of the test function 1 with the ASKA. (a) Iteration 0 (49 samples). (b) Iteration 2 (124 samples). (c) Iteration 10 (462 samples).

where N_1 and N_2 are the values that determine the number of peaks of each function, and the values are 36 and 16, respectively. (x_i, y_i) and (x_k, y_k) are the coordinates of the peaks of each test functions, and a_i, a_k, b_i, and b_k are the values related to the magnitude of peaks. Each value of the parameters are as follows: $a_i = 40$, $b_i = 50(i = \text{odd number})$ or $40(i = \text{even number})$, $a_k = 40$, and $b_k = 60$.

The test was carried out 100 times, and when the error rate of found peak and actual peak is within 5%, the found peak is regarded as success. Figure 10 shows the optimization progress of the ASKA on test function 1. And the average test results are listed in Table 1 and it is obvious that conventional stochastic optimization algorithms require enormous function calls to converge on the accurate peaks. Furthermore, superior performance of ASKA on both computational cost

TABLE 1. Performance comparison of IA, NGA, LHS and ASKA.

Test Function 1 [36 Peaks]	Number of Function call	Success rate [%]
IA	6060	95.75
NGA (RCS)	5840	91.94
LHS	458.0	73.06
ASKA	458.4	99.44
Test Function 2 [16 Peaks]	**Number of Function call**	**Success rate [%]**
IA	5660	93.25
NGA (RCS)	4640	90.63
LHS	286.0	88.56
ASKA	285.9	99.38

and accuracy is validated. The ASKA also shows superior success rate compared with LHS despite the same number of samples.

III. APPLICATION TO THE OPTIMAL DESIGN OF PMa-SynRM FOR EVs

In this section, the ASKA is applied to the optimal design of the PMa-SynRM for EVs. To obtain the precise analysis result, JMAG, which is the commercial FEM analysis tool, is used for analyzing the load condition and no-load condition of the PMa-SynRM. Whenever each sample is added, the structure model is generated with adopted design variables and FEM analysis runs. The overall process of the proposed algorithm is implemented with MATLAB.

A. ANALYSIS MODEL AND DESIGN VARIABLES

For EV propulsion motor, the IPMSM has been widely used, as it has superior performance at the high-speed operation and has advantages of high torque and power density [28]–[30]. However, due to rising price of the rare earth magnets, the PMa-SynRM, in which ferrite magnets are inserted inside rotor core, seems to be good substitute, as it has high efficiency, low cost, and wide range of operating points [31]. The lowered torque by replacing rare earth magnet to ferrite magnet is compensated by applying multi-segmented and multi-layered magnet structure, which allows increased usage of magnet and reluctance torque.

The torque ripple of PMa-SynRM for EVs should have lower torque ripple, as torque ripple produces vibration and noise and results bad control stability and uncomfortable driving [32], [33]. Therefore, the objective function of the optimal design is determined to minimize the torque ripple. For the practical design, the design objectives, such as rated torque, rated output, rated speed, and max speed, are determined according to [34], which is the paper that designs PMa-SynRM for EVs.

The requirements and the parameters of an objective motor are tabulated on Table 2 and Table 3, and the 1/2 periodic analysis model of an objective motor is on Figure 11. As the torque ripple varies according to the shape of the placement of magnets, the design variables are determined as the angle of magnet layer 1, angle, and difference of layer 1 and other

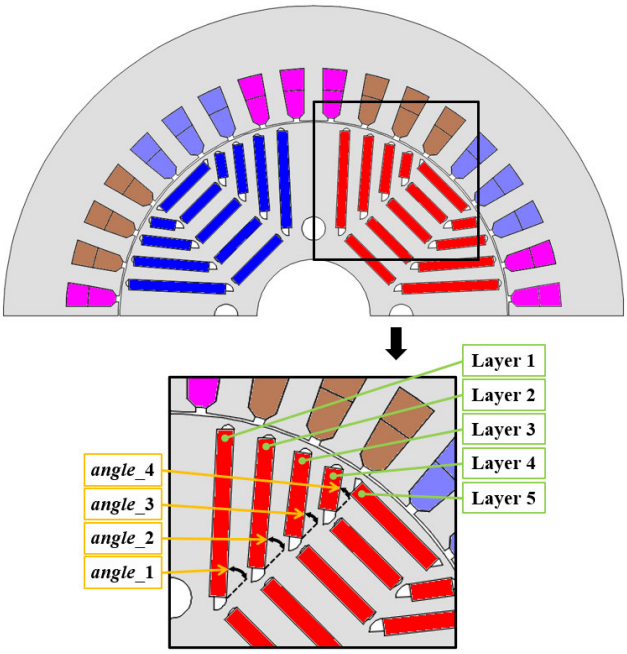

FIGURE 11. 1/2 Periodic analysis model of basic model and design variables.

TABLE 2. Requirements of an objective motor.

Requirement	Value
Rated output	80 [kW]
Rated torque	212.2 [Nm]
Rated / maximum speed	3,600 / 10,000 [rpm]
Torque ripple	Less than 10%

TABLE 3. Specifications of an objective motor.

Parameter	Value
Pole / slot number	4 / 36
Stator inner / outer diameter [mm]	145 / 230
Rotor inner / outer diameter [mm]	42 / 143.8
Air gap [mm]	0.6
Bridge [mm]	1.2
Stacking length [mm]	200
Stator and rotor core material	JFE steel 35PN230
Permanent magnet material	Ferrite 12G (Br=0.44 [T])
Rotor initial degree [degree]	5
Current density [A_{rms}/mm^2]	15.5

magnet layers, difference [35]. The magnet angle of layer 1, 2, 3, and 4 are defined as

$$\begin{aligned} angle\_1 &= angle \\ angle\_2 &= angle\_1 + difference \\ angle\_3 &= angle\_2 + difference \\ angle\_4 &= angle\_3 + difference \end{aligned} \tag{4}$$

where $angle\_1$, $angle\_2$, $angle\_3$, and $angle\_4$ is angle of layer 1 to 4, respectively. The position of magnet of layer 5 is fixed, and the detail range of design variables are specified in Table 4, prohibiting deviation of the magnets from the rotor core and avoiding overlap on each magnet layers. Other values related to the figuration of the PMa-SynRM is fixed,

TABLE 4. Range of design variables.

Variables	Range
angle [degree]	40 to 57
difference [degree]	-5 to 5

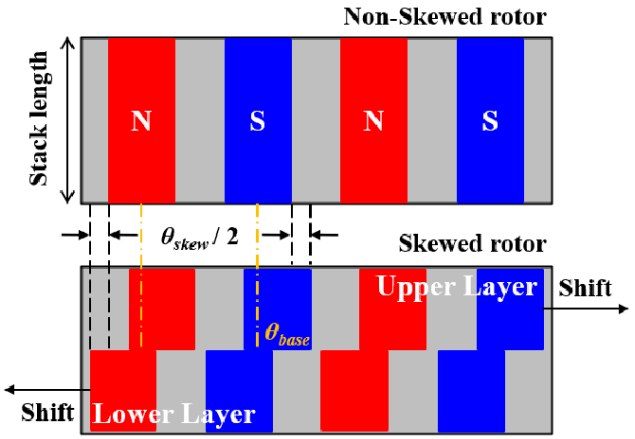

FIGURE 12. Conceptual schematic of skewed rotor.

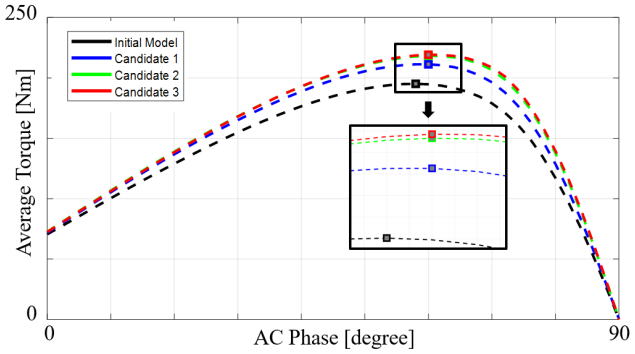

FIGURE 13. Average torque comparison of models at each current phase angle.

and to ensure the mechanical stability, the bridges length and center posts length are stationary. Moreover, whenever the variables change, the average torque changes according to the current phase. Therefore, step that finding current phase with maximum torque is added to the algorithm.

The rotor of the target model has multi-segment and multi-layered permanent magnet structure for the purpose of high efficiency, high power, and high torque density [36]. Moreover, due to the usage of ferrite magnet which has lower magnetic flux density than Nd-Fe-B magnet, the structure of the target model has five layers. Therefore, magnetic saturation of rotor is severe, resulting high pulsation on torque waveform.

To lessen the torque pulsation, noise, and cogging torque, skewed structure is adopted [11], [12]. To simplify the manufacturing process, reduce cost, and reduce the noise and vibration of the motor, two-stepped skewing is applied to rotor [37], [38]. The skew angle can be simply calculated as

$$\frac{360}{LCM(slot, pole)} \cdot \frac{1}{slice} \tag{5}$$

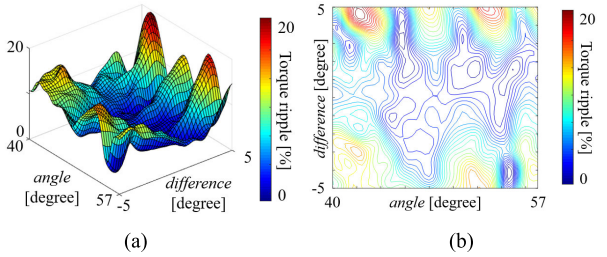

FIGURE 14. Surrogate model of torque ripple of target model. (a) Three-dimension plot. (b) Contour plot.

TABLE 5. Design variables of initial model and candidates.

Model	Initial model	Candidate1	Candidate 2	Candidate 3
angle [degree]	42.39	45.81	50.67	54.19
difference [degree]	-2.05	3.23	3.10	0.85
AC phase [degree]	58	60	60	60

where slot and pole represent the number of slot and pole, and slice means the number of steps. As the target model has 4 pole, 36 slot and two-stepped skew, the skew angle can be calculated as 5°. As shown in Figure 12, half of the skew angle is added or subtracted to upper layer and lower layer. The angle of each layer can be expressed as

$$\begin{aligned} \theta_{up} &= \theta_{base} + \theta_{skew}/2 \\ \theta_{low} &= \theta_{base} - \theta_{skew}/2 \end{aligned} \tag{6}$$

where θ_{up} and θ_{down} are final position of upper and lower layer, θ_{base} is the initial degree of non-skewed model, and θ_{skew} is the determined skew angle.

B. OPTIMAL DESIGN OF PMA-SYNRM EXPLOITING ASKA

The proposed algorithm is applied to optimal design of PMa-SynRM. The objective function of the optimization is torque ripple. Whenever samples are added, on-load FEM analysis is executed. As a result of FEM analysis, a lot of information such as torque ripple, average torque, terminal voltage can be obtained. The total function calls to converges to global and local solutions is 206, and it takes about 20000 minutes.

As a result of optimization, three designs are derived as the local and global minimum solutions of torque ripple. The surrogate model of torque ripple is shown in Figure 14. The design variables of each candidates are shown in Table 5 and the analyzed results of on-load condition and no-load condition of each candidates are listed in Table 6. Optimum model is determined considering other characteristics of each candidates such as average torque, cogging torque, and total harmonic distortion (THD) of line to line back electromotive force (BEMF). As shown in Figure 13, the average torque of each model is selected as the maximum torque considering the current phase angle, and current phase of each models are listed on Table 5. Such current phase finding step is

TABLE 6. Performance comparison of each models.

Model	Initial model	Candidate 1	Candidate 2	Candidate 3
Torque Ripple [%]	13.10	1.99	5.48	2.79
Average Torque [Nm]	195.14	211.28	218.27	219.20
Cogging Torque [mNm]	250.90	480.90	196.34	161.31
THD of the BEMF (Line to line) [%]	4.73	2.34	1.48	1.62

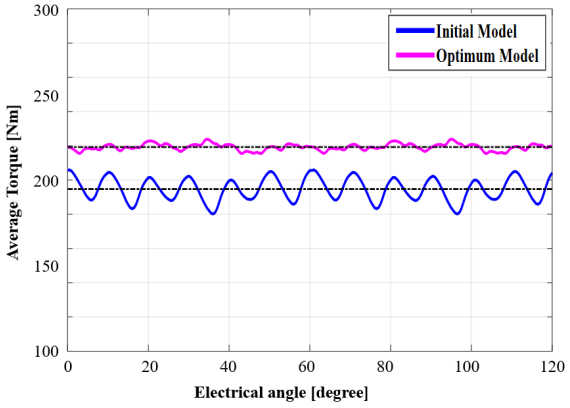

FIGURE 15. Torque waveform of initial model and optimal model.

added to the algorithm and executed whenever the model is changed.

In detail, when it comes to torque ripple, candidate 1 is global solution, which have the lowest torque ripple of all candidates. However, the average torque does not meet the requirement. Moreover, cogging torque and THD of candidate 1 shows highest value among candidates. As both cogging torque and THD have negative effect on motors for EV, candidate 1 was inadequate for optimum model [39], [40]. Candidate 2 shows better performance on cogging torque and THD than candidate 1. However, the torque ripple is highest among three candidates. Although candidate 3 is not global solution on the aspect of torque ripple, average torque is highest compared with other candidates. Also, candidate 3 shows best performance on cogging torque and THD. Therefore, candidate 3 is selected as the optimum model.

C. ANALYSIS OF OPTIMIZATION RESULT

Optimum design with diminished torque ripple is derived throughout applying the ASKA to the optimal design. Figure 15 and Figure 16 show torque and cogging torque pulsation of initial model and optimum model. The average torque of optimum model is 219.20 Nm, which is 12.33% higher than initial model (195.14 Nm). Torque ripple rates 2.49% and decreased by 78.70% of conventional model (13.10%). Cogging torque is 35.71% lessen compared with initial model and rates 0.161 Nm (initial model: 0.251 Nm).

Figure 17 shows magnetic flux density contour plot of optimum model. The magnetic flux density of the most saturated

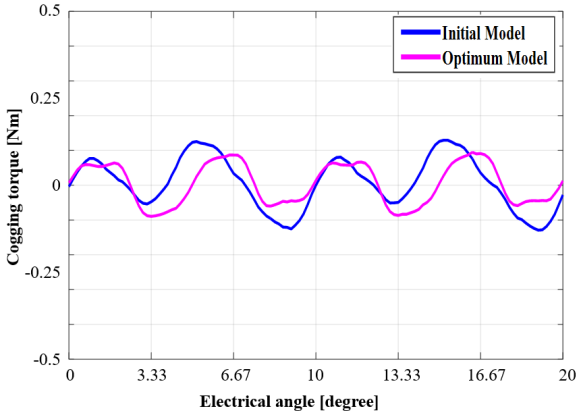

FIGURE 16. Cogging torque waveform of initial model and optimal model.

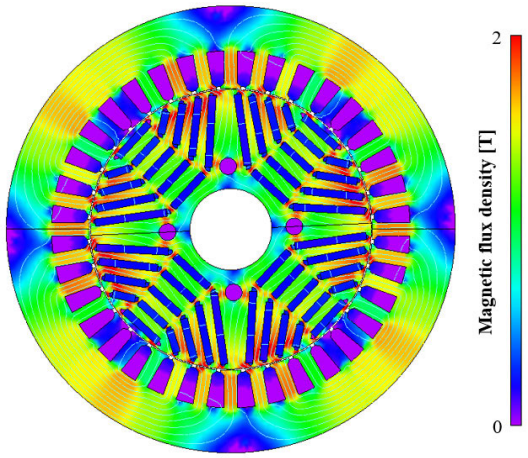

FIGURE 17. Magnetic flux density contour of optimal model.

TABLE 7. Power characteristic of initial model and optimum model.

Model	Initial model	Optimum model
Iron loss [W]	326.09	312.02
Copper loss [W]	3309.24	3309.24
Total loss [W]	3635.24	3621.27
Input power [kW]	77.17	86.24
Output power [kW]	73.53	82.62
Efficiency [%]	95.3	95.8

point of initial model and optimum model are 2.45 T and 2.48 T, respectively. Power characteristics of both models are tabulated on Table 7 and optimum model shows little bit higher efficiency.

When performing the optimal design, the length of the bridge and the center posts of each magnet layers were fixed to ensure mechanical stability [41], [42]. However, as motors for EV propulsion operate on various speed range, especially at high speed, the analysis of mechanical stress at maximum speed is essential. In case of the motors that magnets are embedded inside rotor, maximum mechanical stress is applied to the center post and the bridge, which are the most vulnerable points for breakage on the high-speed rotation [43], [44]. Table 8 shows parameters for the mechanical

TABLE 8. Parameters for the mechanical stress analysis.

Parameter	Value
Young's modulus (Core / Ferrite)	210 / 190 [GPa]
Poisson's ratio (Core / Ferrite)	0.3 / 0.35
Density (Core / Ferrite)	7,850 / 5,100 [kg/m3]
Rotation Speed	3,600 / 10,000 [rpm]
Yield stress	250 [MPa]

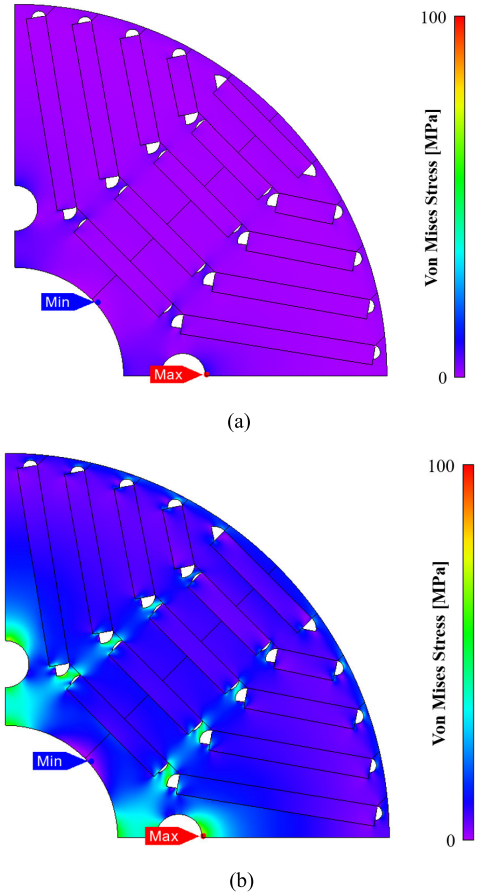

FIGURE 18. Von mises stress analysis result of the optimum model. (a) Rated speed. (b) Maximum speed.

stress analysis, and maximum speed is set as 10,000 rpm. Figure 18 shows the mechanical stress analysis result of the optimum model and the maximum Von Mises stress of rated speed and maximum speed are 11.76 MPa and 90.74 MPa, respectively. Therefore, it can be said that the optimum model is safe from breakage at maximum speed, as its maximum mises stress does not exceed the yield stress value of 250 MPa.

IV. CONCLUSION

This paper proposes the ASKA for solving multi-modal optimization problem. With usage of contour information, the kriging surrogate model with effectively generated samples could find global and local solutions with reduced function calls. Such an enormous save on computational cost make the ASKA particularly appropriate for the optimal design of electrical machines exploiting FEM analysis. Verification of superior performance of the proposed algorithm is done by applying the ASKA, other kriging-based algorithm, and conventional algorithms such as IA and NGA to the mathematical test functions. Moreover, the optimal design of PMa-SynRM for EV propulsion motor, where design objective is diminishing torque ripple, is derived throughout combination of the ASKA and the FEM, and the computational cost could be tremendously saved.

REFERENCES

[1] J.-H. Seo, D.-K. Woo, T.-K. Chung, and H.-K. Jung, "A study on loss characteristics of IPMSM for FCEV considering the rotating field," *IEEE Trans. Magn.*, vol. 46, no. 8, pp. 3213–3216, Aug. 2010.
[2] Z. Chen and G. Li, "A V type permanent magnet motor simulation analysis and prototype test for electric vehicle," *IEEE Access*, vol. 7, pp. 174839–174846, Dec. 2019.
[3] N. Bianchi, E. Fornasiero, M. Ferrari, and M. Castiello, "Experimental comparison of PM-assisted synchronous reluctance motors," *IEEE Trans. Ind. Appl.*, vol. 52, no. 1, pp. 163–171, Jan. 2016.
[4] H.-C. Liu, I.-G. Kim, Y. J. Oh, J. Lee, and S.-C. Go, "Design of permanent magnet-assisted synchronous reluctance motor for maximized back-EMF and torque ripple reduction," *IEEE Trans. Magn.*, vol. 53, no. 6, pp. 1–4, Jun. 2017.
[5] M. Amin and G. A. A. Aziz, "Hybrid adopted materials in permanent magnet-assisted synchronous reluctance motor with rotating losses computation," *IEEE Trans. Magn.*, vol. 55, no. 6, pp. 1–5, Jun. 2019.
[6] C.-T. Liu, T.-Y. Luo, P.-C. Shih, S.-C. Yen, H.-N. Lin, Y.-W. Hsu, and C.-C. Hwang, "On the design and construction assessments of a permanent-magnet-assisted synchronous reluctance motor," *IEEE Trans. Magn.*, vol. 53, no. 11, pp. 1–4, Nov. 2017.
[7] W.-H. Kim, K.-S. Kim, S.-J. Kim, D.-W. Kang, S.-C. Go, Y.-D. Chun, and J. Lee, "Optimal PM design of PMA-SynRM for wide constant-power operation and torque ripple reduction," *IEEE Trans. Magn.*, vol. 45, no. 10, pp. 4660–4663, Oct. 2009.
[8] H.-S. Kim and B.-I. Kwon, "Optimal design of motor shape and magnetization direction to obtain vibration reduction and average torque improvement in IPM BLDC motor," *IET Electr. Power Appl.*, vol. 11, no. 3, pp. 378–385, Mar. 2017.
[9] J.-G. Lee, D.-K. Lim, and H.-K. Jung, "Analysis and design of interior permanent magnet synchronous motor using a sequential-stage magnetic equivalent circuit," *IEEE Trans. Magn.*, vol. 55, no. 10, pp. 1–4, Oct. 2019.
[10] D.-K. Lim, D.-K. Woo, H.-K. Yeo, S.-Y. Jung, J.-S. Ro, and H.-K. Jung, "A novel surrogate-assisted multi-objective optimization algorithm for an electromagnetic machine design," *IEEE Trans. Magn.*, vol. 51, no. 3, pp. 1–4, Mar. 2015.
[11] D. Torregrossa, F. Peyraut, M. Cirrincione, C. Espanet, A. Cassat, and A. Miraoui, "A new passive methodology for reducing the noise in electrical machines: Impact of some parameters on the modal analysis," *IEEE Trans. Ind. Appl.*, vol. 46, no. 5, pp. 1899–1907, Sep. 2010.
[12] Y. Kawase, T. Yamaguchi, Z. Tu, N. Toida, N. Minoshima, and K. Hashimoto, "Effects of skew angle of rotor in squirrel-cage induction motor on torque and loss characteristics," *IEEE Trans. Magn.*, vol. 45, no. 3, pp. 1700–1703, Mar. 2009.
[13] H.-K. Yeo, D.-K. Lim, D.-K. Woo, J.-S. Ro, and H.-K. Jung, "Magnetic equivalent circuit model considering overhang structure of a surface-mounted permanent-magnet motor," *IEEE Trans. Magn.*, vol. 51, no. 3, pp. 1–4, Mar. 2015.
[14] J. H. Lee, J.-W. Kim, J.-Y. Song, D.-W. Kim, Y.-J. Kim, and S.-Y. Jung, "Distance-based intelligent particle swarm optimization for optimal design of permanent magnet synchronous machine," *IEEE Trans. Magn.*, vol. 53, no. 6, pp. 1–4, Jun. 2017.
[15] M. Khaleghi, M. M. Farsangi, H. Nezamabadi-pour, and K. Y. Lee, "Pareto-optimal design of damping controllers using modified artificial immune algorithm," *IEEE Trans. Syst., Man, Cybern. C, Appl. Rev.*, vol. 41, no. 2, pp. 240–250, Mar. 2011.
[16] J.-T. Tsai and J.-H. Chou, "Design of optimal digital IIR filters by using an improved immune algorithm," *IEEE Trans. Signal Process.*, vol. 54, no. 12, pp. 4582–4596, Dec. 2006.
[17] D.-H. Cho, H.-K. Jung, T.-K. Chung, and C.-G. Lee, "Design of a short-time rating interior permanent magnet synchronous motor using a niching genetic algorithm," *IEEE Trans. Magn.*, vol. 36, no. 4, pp. 1936–1940, Jul. 2000.

[18] D.-H. Cho, J.-K. Kim, H.-K. Jung, and C.-G. Lee, "Optimal design of permanent-magnet motor using autotuning niching genetic algorithm," *IEEE Trans. Magn.*, vol. 39, no. 3, pp. 1265–1268, May 2003.
[19] D.-K. Lim, D.-K. Woo, I.-W. Kim, J.-S. Ro, and H.-K. Jung, "Cogging torque minimization of a dual-type axial-flux permanent magnet motor using a novel optimization algorithm," *IEEE Trans. Magn.*, vol. 49, no. 9, pp. 5106–5111, Sep. 2013.
[20] G. Lei, K. R. Shao, Y. Guo, J. Zhu, and J. D. Lavers, "Sequential optimization method for the design of electromagnetic device," *IEEE Trans. Magn.*, vol. 44, no. 11, pp. 3217–3220, Nov. 2008.
[21] D.-K. Lim, K.-P. Yi, S.-Y. Jung, H.-K. Jung, and J.-S. Ro, "Optimal design of an interior permanent magnet synchronous motor by using a new surrogate-assisted multi-objective optimization," *IEEE Trans. Magn.*, vol. 51, no. 11, pp. 1–4, Nov. 2015.
[22] J.-C. Yu and Suprayitno, "Evolutionary reliable regional Kriging surrogate and soft outer array for robust engineering optimization," *IEEE Access*, vol. 5, pp. 16520–16531, Aug. 2017.
[23] S. Xiao, M. Rotaru, and J. K. Sykulski, "Robust design optimisation of electromagnetic devices exploiting gradient indices and Kriging," *IET Sci., Meas. Technol.*, vol. 9, no. 4, pp. 400–409, Jul. 2015.
[24] B. Xia, T.-W. Lee, K. Choi, and C.-S. Koh, "A novel adaptive dynamic Taylor Kriging and its application to optimal design of electromagnetic devides," *IEEE Trans. Magn.*, vol. 52, no. 3, pp. 1–4, Mar. 2016.
[25] W.-C. Yeh, J. C. P. Su, T.-J. Hsieh, M. Chih, and S.-L. Liu, "Approximate reliability function based on wavelet latin hypercube sampling and bee recurrent neural network," *IEEE Trans. Rel.*, vol. 60, no. 2, pp. 404–414, Jun. 2011.
[26] *The Mathworks Inc*. [Online]. Available: http://www.mathworks.com/help/techdoc/ref/contour.html
[27] H. You, M. Yang, D. Wang, and X. Jia, "Kriging model combined with latin hypercube sampling for surrogate modeling of analog integrated circuit performance," in *Proc. 10th Int. Symp. Qual. Electron. Design*, San Jose, CA, USA, Mar. 2009, pp. 554–558.
[28] H. Chen and C. H. T. Lee, "Parametric sensitivity analysis and design optimization of an interior permanent magnet synchronous motor," *IEEE Access*, vol. 7, pp. 159918–159929, Nov. 2019.
[29] J. Hao, S. Suo, Y. Yang, Y. Wang, W. Wang, and X. Chen, "Optimization of torque ripples in an interior permanent magnet synchronous motor based on the orthogonal experimental method and MIGA and RBF neural networks," *IEEE Access*, vol. 8, pp. 27202–27209, Feb. 2020.
[30] J. Sun, X. Luo, and X. Ma, "Realization of maximum torque per ampere control for IPMSM based on inductance segmentation," *IEEE Access*, vol. 6, pp. 66088–66094, Oct. 2018.
[31] F. Xing, W. Zhao, and B. Kwon, "Design and optimisation of a novel asymmetric rotor structure for a PM assisted synchronous reluctance machine," *IET Electr. Power Appl.*, vol. 13, no. 5, pp. 573–580, May 2019.
[32] Y. Kong, M. Lin, M. Yin, and L. Hao, "Rotor structure on reducing demagnetization of magnet and torque ripple in a PMa-synRM with ferrite permanent magnet," *IEEE Trans. Magn.*, vol. 54, no. 11, pp. 1–5, Nov. 2018.
[33] W. Ren, Q. Xu, Q. Li, and L. Zhou, "Reduction of cogging torque and torque ripple in interior PM machines with asymmetrical V-Type rotor design," *IEEE Trans. Magn.*, vol. 52, no. 7, pp. 1–5, Jul. 2016.
[34] Y.-H. Jeong, K. Kim, Y.-J. Kim, B.-S. Park, and S.-Y. Jung, "Design characteristics of PMa-SynRM and performance comparison with IPMSM based on numerical analysis," in *Proc. 20th Int. Conf. Electr. Mach.*, Marseille, France, Sep. 2012, pp. 164–170.
[35] L. Fang, S.-I. Kim, S.-O. Kwon, and J.-P. Hong, "Novel double-barrier rotor designs in interior-PM motor for reducing torque pulsation," *IEEE Trans. Magn.*, vol. 46, no. 6, pp. 2183–2186, Jun. 2010.
[36] D.-K. Lim, K.-P. Yi, D.-K. Woo, H.-K. Yeo, J.-S. Ro, C.-G. Lee, and H.-K. Jung, "Analysis and design of a multi-layered and multi-segmented interior permanent magnet motor by using an analytic method," *IEEE Trans. Magn.*, vol. 50, no. 6, pp. 1–8, Jun. 2014.
[37] J.-W. Jung, D.-J. Kim, J.-P. Hong, G.-H. Lee, and S.-M. Jeon, "Experimental verification and effects of step skewed rotor type IPMSM on vibration and noise," *IEEE Trans. Magn.*, vol. 47, no. 10, pp. 3661–3664, Oct. 2011.
[38] J. Bao, B. L. J. Gysen, K. Boynov, J. J. H. Paulides, and E. A. Lomonova, "Torque ripple reduction for 12-stator/10-rotor-pole variable flux reluctance machines by rotor skewing or rotor teeth non-uniformity," *IEEE Trans. Magn.*, vol. 53, no. 11, Nov. 2017, Art. no. 8111405.
[39] D.-W. Kim, G.-J. Park, J.-H. Lee, J.-W. Kim, Y.-J. Kim, and S.-Y. Jung, "Hybridization algorithm of fireworks optimization and generating set search for optimal design of IPMSM," *IEEE Trans. Magn.*, vol. 53, no. 6, pp. 1–4, Jun. 2017.
[40] A. S. Evans, "Salient pole shoe shapes of interior permanent magnet synchronous machines," in *Proc. 19th Int. Conf. Electr. Mach. (ICEM)*, Rome, Italy, Oct. 2010, pp. 1–6.
[41] Y.-R. Kang, J.-C. Son, and D.-K. Lim, "Optimal design of IPMSM for fuel cell electric vehicles using autotuning elliptical niching genetic algorithm," *IEEE Access*, vol. 8, pp. 117405–117412, Jun. 2020.
[42] J.-C. Son, Y.-R. Kang, and D.-K. Lim, "Optimal design of IPMSM for FCEV using novel immune algorithm combined with steepest descent method," *Energies*, vol. 13, no. 13, p. 3395, Jul. 2020.
[43] G. Chu, R. Dutta, F. M. Rahman, H. Lovatt, and B. Sarlioglu, "Analytical calculation of maximum mechanical stress on the rotor of interior permanent-magnet synchronous machines," *IEEE Trans. Ind. Appl.*, vol. 56, no. 2, pp. 1321–1331, Mar./Apr. 2020.
[44] F. Chai, Y. Li, P. Liang, and Y. Pei, "Calculation of the maximum mechanical stress on the rotor of interior permanent-magnet synchronous motors," *IEEE Trans. Ind. Electron.*, vol. 63, no. 6, pp. 3420–3432, Jun. 2016.

JI-CHANG SON received the B.S. degree in electrical engineering from the School of Electrical Engineering, University of Ulsan, South Korea, in 2019, where he is currently pursuing the M.S. degree.

His research interests include analysis and optimal design of electrical machines.

JONG-MIN AHN received the B.S. degree in electrical engineering from the School of Electrical Engineering, University of Ulsan, South Korea, in 2020, where he is currently pursuing the M.S. degree.

His research interests include analysis and optimal design of electrical machines.

JAEWON LIM (Member, IEEE) received the B.S., M.S., and Ph.D. degrees in electrical and computer engineering from Seoul National University, in 2004, 2006, and 2011, respectively. Since 2011, he has been a Senior Researcher with the Korea Institute of Machinery and Materials (KIMM). His research interests include design of magnetic actuator and linear propulsion systems.

DONG-KUK LIM (Member, IEEE) received the B.S. degree in electrical engineering from Dongguk University, Seoul, South Korea, in 2010, and the Ph.D. degree in electrical engineering from Seoul National University, Seoul, in 2017, through the combined master's and doctorate program.

In 2017, he was with the Electrical Power Engineering Team, Hyundai Mobis Company, South Korea, as a Senior Research Engineer. He is currently an Assistant Professor with the School of Electrical Engineering, University of Ulsan, South Korea. His research interests include analysis and optimal design of electrical machines.